Spontaneous hot-carrier photon emission rates in silicon: Improved modeling and applications to metal oxide semiconductor devices

M. Pavesi, P. L. Rigolli, and M. Manfredi
Department of Physics, University of Parma and INFM, Parco Area delle Scienze 7/A, 43100 Parma, Italy

P. Palestri and L. Selmi
DIEGM, Department of Electrical, Mechanical and Management Engineering, University of Udine, via delle Scienze 208, 33100 Udine, Italy

(Received 12 October 2001; published 8 May 2002)

The recent publication of controversial experimental evidence on the origin of hot-carrier currents in 4–10 nm tunnel metal oxide semiconductor capacitors renewed the interest in improving hot-carrier luminescence models for silicon devices. This work presents several such improvements, aimed at making possible a physically based analysis of the hot-carrier luminescence effects taking place during tunneling experiments in relatively thick SiO_2 layers. To this purpose, silicon band structure and scattering rate calculations have been extended well above 10 eV by considering eight conduction bands, instead of the usual four, so as to allow for a detailed description of the high-energy carriers injected from silicon into silicon dioxide during tunneling experiments. The absolute contributions of the direct and phonon-assisted, interband and intraband transitions of electrons and holes to the total photon emission rate are analyzed, so the results can be directly compared with the experimental data. To the best of our knowledge, it is for the first time that results for valence-to-valence band transitions of holes are presented and compared with those of conduction-to-conduction band transitions of electrons. Results can be directly compared with experimental data. Template results obtained with a variety of carrier distributions (Maxwellian, Gaussian, and Dirac's delta-like) are shown and implications for device analysis are discussed.

DOI: 10.1103/PhysRevB.65.195209 PACS number(s): 71.15.−m, 72.10.−d, 78.20.−e

I. INTRODUCTION

The majority carrier substrate current I_{Smaj}, the gate current I_G, and the hot-carrier luminescence intensity I_L, experimentally observed in metal oxide semiconductor (MOS) transistors biased in the saturation region,[1,2] as well as in MOS capacitors biased in the tunneling regime,[3–5] represent important and complementary monitors to predict device degradation and reliability of advanced metal oxide semiconductor field effect transistors (MOSFET's) and nonvolatile memory cells.[6–8] I_{Smaj}, produced by the generation of positive charge during electron injection,[9,10] is also a key parameter to monitor the reliability of tunneling MOS capacitors because, according to the widely accepted anode hole injection (AHI) model,[11,12] degradation and breakdown of thin SiO_2 layers are more or less tightly related to the fluence through the oxide (Q_p) of holes generated by impact ionization (II) of tunneling electrons and injected back into the oxide at the anode. This fluence is assumed to be measurable as $Q_p=\int I_{Smaj}dt$ (see Fig. 1).

An additional minority carrier substrate current I_{Smin} can be measured during hot-carrier and tunneling experiments on MOS devices, if a slightly reverse biased collecting junction is available in the neighborhood of the device.[13] Originally attributed to the diffusion of secondary carriers generated by II from the MOS depletion layer towards the quasineutral substrate,[14] I_{Smin} is nowadays generally ascribed to the reabsorption of near-band-gap photons emitted by the hot carriers.[15–17]

Recent experimental evidences on the correlation between I_{Smaj} and I_{Smin} in 4 to 9 nm SiO_2 layers led Rasras *et al.*[6] to question the validity of the AHI model-based interpretation of I_{Smaj}, and to propose that the majority carrier substrate current measured in tunneling *n*-MOS capacitors at positive gate voltages (V_G) could actually be the result of photon emission processes as those illustrated in Fig. 1. If confirmed, this result will have important consequences on the validity of AHI models of device degradation, hence on reliability assessment procedures.

The interpretation of these results, however, is based on comparison with crude empirical or analytical models,[18] hardly applicable to the problem at hand. In order to shed light on these complex phenomena, refined calculations of hot-carrier-induced photon emission (PE) spectra in silicon are thus highly valuable.

Bude *et al.*[19] performed numerical calculations of sponta-

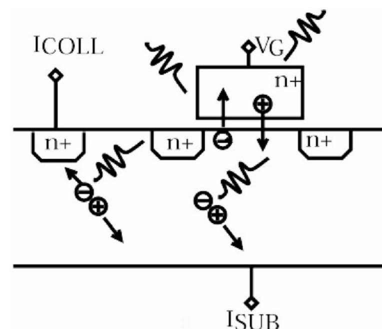

FIG. 1. Schematic representation of hot-carrier phenomena taking place in tunneling MOS capacitors.

 ©2002 The American Physical Society

neous PE rates in silicon. Their theoretical model, based on a local silicon band structure, provides the PE spectra for conduction-to-conduction (c-c) and conduction-to-valence (c-v) direct and indirect [phonon assisted (PA) and impurity assisted (IA)] radiative transitions. Villa *et al.*[20] improved the calculations with the introduction of a finite lifetime of the intermediate state in the second-order transitions and by using a more realistic photon density of states that takes into account the photon energy dependence of the dielectric function. Unfortunately, none of these models is fully suited to analyze hot-carrier effects in the relatively thick MOS capacitors of Ref. 6.

First, the density of states only extends up to approximately 6 eV, while significantly higher-energy carriers are injected in silicon during tunneling experiments on 4–10 nm MOS capacitors. Moreover, since both hot electrons and hot holes are simultaneously present in a tunneling experiment, then the contribution of both carriers should be included in the model. Finally, none of these papers presents PE rates in absolute units, i.e., suited to compute the actual photon flux per unit energy and volume, hence the number of carrier pairs generated by the reabsorption of photons in the substrate.

In this paper we address all these points by reporting further improvements in hot-carrier-induced PE modeling in silicon. In particular, we first applied the nonlocal (NL) empirical pseudopotential method (EPM) to compute four additional conduction bands, thus extending the description of the silicon band structure well above 10 eV, and verified the results with those given by first-principle techniques.[21] Furthermore, PE rates due to v-v band transitions of holes have been calculated and compared to those of c-c and c-v mechanisms. PE rates in absolute units are given and the contributions of the different phonons are shown. The calculus program was first tested with Maxwellian, Gaussian, and Dirac's delta-like carrier distributions.

These improvements in the PE model allowed us to carry out a detailed analysis of the experiments of Ref. 6, leading to the conclusion that PE cannot explain the measured substrate current of moderately thick oxides.[22]

II. THEORETICAL PLANNING AND COMPUTATIONAL MODEL

A. Extended-band-structure calculations

The NL-EPM employed to calculate the electronic structure of silicon makes use of the empirical pseudopotential factors given in Ref. 23. The pseudo-wave-functions are depicted as an expansion on a plane-wave set and, at every **k** point, the number of plane waves is fixed by a cut-off energy. The more convenient value for the cut-off energy was found to be 10 Ry since higher values only lead to add negligible terms to pseudo-wave-functions and to slight corrections (a few meV) in the Hamiltonian eigenvalues.

The conduction band structure was extended well above 10 eV (zero energy was taken at the bottom of the conduction band) by considering 12 bands—four valence bands and eight conduction bands—instead of the usual four. A regular cubic mesh in the **k** space was employed featuring up to 80 divisions ($n_{div}=20$, 40, or 80) between Γ and L points in the Brillouin zone (BZ); this is equivalent to 916, 6281, and 46361 points, respectively, in the irreducible wedge (IW) in a cubic mesh arrangement. The results were verified to be independent of the grid size.

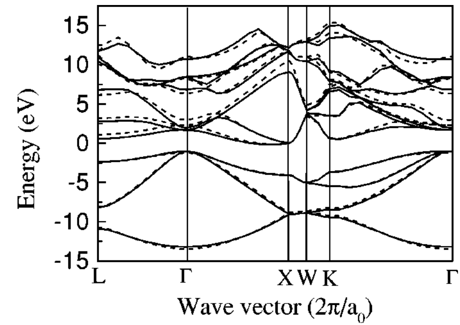

FIG. 2. Silicon band structure calculated by NL-EPM (solid line) and FP (dashed line) methods ($n_{div}=80$).

As shown in Fig. 2, the calculated band structure, and then the density of states (DoS), are in good agreement with that derived from *ab initio* calculations performed in the density-functional theory by means of the package FHI96MD.[24] This code employs first-principles atomic pseudopotentials, generated by the package FHI98PP,[26] and a plane-wave basis set. For the exchange and correlation terms both the local density and the generalized gradient approximations (LDA and GGA) are used. In Fig. 2 we report only results for the LDA. The total energy minimum was found after electronic and ionic minimization and band structure was computed by over 64 **k** points[25] in a fcc primitive cell by keeping the cut-off energy at 24 Ry. More details on the band-structure calculations and features will be given in Ref. 21.

B. General features of the PE model

The PE rates have been computed treating the electromagnetic field as a classic field and the force over the charge as an external force, so that the wave-packet solutions of the Schrödinger equation follow the same trajectories as a classical particle obeying the equations of motion derived from the corresponding classical Hamiltonian. In this context, the spontaneous PE rate R, defined as the number of photons per energy, volume, solid angle and time units, is calculated by the Fermi golden rule for direct and PA mechanisms.

Since in MOS devices IA transitions are relevant sources of photons only at very high impurity concentrations,[19,27–31] we did not consider this PE mechanism in our model.

C. Direct transitions

Direct radiative transitions lead to the generation of photons with energy $\hbar\omega = E_u - E_l$, i.e., the difference between the initial (E_u) and final (E_l) carrier energies. The transition is almost vertical in the **k** space, because of the very small photon kinetic momentum.

The spontaneous photon emission probability per unit time $W_{lu}^{D}(\hbar\omega)$ between the initial state u and the final state l at the **k** point in the BZ is given by the Fermi golden rule

$$W_{lu}^{D}(\hbar\omega)=\frac{2\pi}{\hbar}|H_{lu}^{ef}|^{2}\delta(E_{u}(\mathbf{k})-E_{l}(\mathbf{k})-\hbar\omega), \quad (1)$$

where $H_{lu}^{ef}=\langle l|H^{ef}|u\rangle$ is the direct matrix element calculated as the expectation value of the Hamiltonian over the initial (u) and final (l) state pseudo-wave-functions. The H^{ef} is the electron-photon Hamiltonian given by the radiation field theory,[19]

$$H^{ef}=-\frac{i\hbar e}{m_0}\sqrt{\frac{\hbar}{2V\omega\epsilon_0\epsilon}}e^{i\mathbf{q}\cdot\mathbf{r}}\mathbf{e}_{\lambda}\cdot\nabla_{\mathbf{r}} \quad (2)$$

and $\mathbf{e}_{\lambda}$ is the photon polarization direction, $\mathbf{q}\approx\mathbf{0}$ is the kinetic momentum of the photon, ρ is the silicon mass density, $\epsilon=\epsilon(0,\omega)$ is the dynamic dielectric function at $\mathbf{k}=\mathbf{0}$, ϵ_0 is the static dielectric function, V is the sample volume, m_0 and e are the electron rest mass and charge, respectively.

The direct PE rate $R_{dir}(\hbar\omega)$ in units of photons/(eV s m^{3}str) is then computed multiplying W_{lu}^{D} by the occupation function $f(E)$ of the initial and final states, by the optical density of states G_{opt} and summing over all the initial and final states of a suitable mesh of $\mathbf{k}$ points in the BZ. The resulting expression of R_{dir} per unit solid angle is

$$R_{dir}(\hbar\omega)=\frac{s}{(2\pi)^3}\int d\mathbf{k}\sum_{lu} W_{lu}^{D}G_{opt}f_u\bar{f}_l, \quad (3)$$

where $\bar{f}_l=1-f_l$ and the multiplicative factor $s/(2\pi)^3$ takes into account the spin degeneracy s, and the $\mathbf{k}$-space density of states. $G_{opt}(\hbar\omega)$ is the vibration mode number per unit energy for a polarization direction computed as in Ref. 20, i.e., accounting for the photon energy dependence of the dielectric function,

$$G_{opt}=\frac{V}{(2\pi)^3}\frac{\omega^2\epsilon^{3/2}}{\hbar c^3}\left|1+\frac{\omega}{\sqrt{\epsilon}}\frac{d\sqrt{\epsilon}}{d\omega}\right|. \quad (4)$$

D. PA indirect transitions

Phonon-assisted transitions involve an additional particle (phonon) so that the spontaneous PE probability has to be treated according to the second-order perturbation theory. The PE probability for absorption/emission of one phonon type becomes

$$W_{lu}^{PA}(\hbar\omega)=\frac{2\pi}{\hbar}\left[\sum_{m}\left|\frac{H_{um}^{ef}(H_{ml}^{ep})_{\pm}}{E_u-E_m-\hbar\omega+i\Gamma_{\omega}}\right|^2+\sum_{m'}\left|\frac{(H_{um'}^{ep})_{\pm}H_{m'l}^{ef}}{E_{m'}-E_l-\hbar\omega+i\Gamma_{\omega}}\right|^2\right]\delta(E_u(\mathbf{k}\pm\mathbf{q})-E_l(\mathbf{k})-\hbar\omega\pm\hbar\omega_p), \quad (5)$$

where H^{ep} is the electron-phonon Hamiltonian, H_{um}^{ef} and $H_{m'l}^{ef}$ are the direct matrix elements calculated as in Eq. (1), $\hbar\omega_p$ is the phonon energy, $\mathbf{q}=\mathbf{k}-\mathbf{k}'$ is the phonon kinetic momentum, m is the so-called "virtual state," and Γ_{ω} is the self-energy.

The electron-phonon Hamiltonians for optical and acoustic phonons are

$$H^{ep,opt}=\sqrt{\frac{\hbar(n_q+1)}{2\rho V\omega_p}}\Delta_{opt}e^{i\mathbf{q}\cdot\mathbf{r}}, \quad (6)$$

$$H^{ep,ac}=\sqrt{\frac{K_BT}{2\rho Vv_s^2}}\Delta_{ac}e^{i\mathbf{q}\cdot\mathbf{r}}, \quad (7)$$

where $\mathbf{q}$ is the exchanged momentum, n_q is the phonon occupation number, Δ_{opt} and Δ_{ac} are the deformation potentials for optical and acoustic phonons, respectively, v_s is the sound velocity in silicon, and ω_q is the phonon frequency.

According to Eq. (5) the second-order transition is split in a momentum-conserving photon-assisted vertical transition between the initial state u, and an intermediate state m, and a momentum nonconserving transition between the intermediate and the final state. Energy conservation is enforced only over the whole transition; a symmetric process in which the electron-phonon interaction precedes the electron-photon one was also considered.

Following Ref. 20 we introduced a self-energy factor $\Gamma_{\omega}=\hbar/2\tau$ to avoid divergent terms in the summation of Eq. (3), where τ is the total scattering rate[19] (including II and phonon scattering) calculated on the same full band structure used for PE calculations. Summation over all possible initial, final, and intermediate states yields the total indirect photon emission rate $R_{PA}(\hbar\omega)$ per unit of solid angle,

$$R_{PA}(\hbar\omega)=V\int_{BZ}d\mathbf{k}\frac{s}{(2\pi)^3}\int_{BZ}d\mathbf{k}'\frac{1}{(2\pi)^3}\times\sum_{lu} W_{lu}^{PA}G_{opt}f_u\bar{f}_l. \quad (8)$$

The intermediate states are chosen inside the completeness of the Hamiltonian eigenvalues accounting for the occupation probability.

E. Model implementation

Equations (3) and (8) were numerically implemented as follows.

Integrals over the BZ were reduced within the IW exploiting the 48-fold symmetry of the silicon band structure and the integration over the $\mathbf{k}$ space was replaced with a summation over $\mathbf{k}$ points at the vertices of a regular grid of discrete cubes in the IW. The discretization step is $\Delta k=2\pi/a_0n_{div}$, where a_0 is the lattice constant. Replacement of the $\mathbf{k}$-space integral with the summation yields

$$\int\delta(E-E_0)d\mathbf{k}=\sum_{\mathbf{k}=\mathbf{k}(E_0)}\frac{(\Delta k)^3}{\Delta E}, \quad (9)$$

where the factor $1/\Delta E$ stems from the energy conservation law

$$\delta(E-E_0)=\begin{cases}1/\Delta E, & |E-E_0|\leqslant\Delta E/2\\ 0, & \text{otherwise,}\end{cases} \quad (10)$$

ΔE is taken equal to the distribution function discretization step (typically $\Delta E = 0.05$ eV).

k points at the edge of the IW were weighted by an appropriate factor w accounting for BZ symmetry.

As for the indirect PE rate, the double integration over **k** space is performed with the same algorithm discussed above. However, in order to speed up the summation process, two different grids of **k** points were used: one for the electron-photon interaction and a coarser one for the electron-phonon interaction (typically $n_{div} = 40$ in the former, $n_{div} = 20$ in the latter). Indeed, since the electron-phonon interaction is characterized by higher values of exchanged momentum than the electron-photon one, a coarser grid can be used without loss of accuracy. Calculations performed by using two identical grids demonstrated the validity of this approach.

The matrix elements in Eqs. (1) and (5) are evaluated inside each cube of the mesh and are expressed in $2\pi/a_0$ units; hence, the square operation in Eqs. (1) and (5) introduces the term $(2\pi/a_0)^2$. Neglecting the polarization of the emitted light, an additional factor $(1/\sqrt{3})^2$ is included to account for the average over all photon polarizations.[20]

The optical density of states $G_{opt}(\hbar\omega)$ takes into account the dependence of the dielectric function ϵ on the photon energy.[20] The dielectric function data were taken from Ref. 31. The phonon model (acoustic and optical) is the same as the full band Monte Carlo code of Ref. 22 and was calibrated by means of comparison with mobility, drift velocity, impact ionization and gate current data. The PE model is thus fully consistent with the full band structure and scattering rates used to analyze the device behavior.

The degeneracy factor s is 4 for both direct and indirect transitions: the spin of the initial energy level weights for a factor 2, and another factor 2 comes from the transverse polarizations of the emitted photon.

We can put together all previous factors by defining two multiplicative constant Γ_{dir} and Γ_{PA} as

$$\Gamma_{dir} = \left(\frac{2\pi}{a_0 n_{div}}\right)^3 \left(\frac{2\pi}{a_0}\right)^2 \left(\frac{1}{2\pi}\right)^3 \frac{s}{\Delta E} C \tag{11}$$

$$\Gamma_{PA} = \left(\frac{2\pi}{a_0 \times N_{div}}\right)^3 \left(\frac{2\pi}{a_0 \times n_{div}}\right)^3 \left(\frac{2\pi}{a_0}\right)^2 \left(\frac{1}{2\pi}\right)^6 \frac{s}{\Delta E} C \tag{12}$$

where $C = \frac{48}{3}(e^2/8\pi^2 m_0^2 c^3 \epsilon_0)$, N_{div} is the number of divisions for the grid used in the electron-phonon iteration and the term $(1/2\pi)^3$ is the **k**-space density of states. The final forms for R_{dir} and R_{PA} are

$$R_{dir} = \Gamma_{dir} \sum_{\mathbf{k} \in IW} w \sum_{l,u,i} \hbar\omega |\langle l|\nabla_i|u\rangle|^2 \sqrt{\epsilon} \left| 1 + \frac{\omega}{\sqrt{\epsilon}} \frac{d\sqrt{\epsilon}}{d\omega} \right| f_u \bar{f}_l, \tag{13}$$

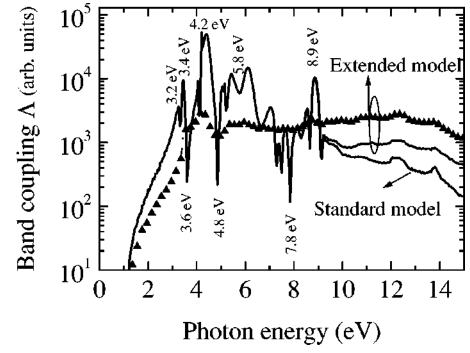

FIG. 3. Band-coupling term Λ: extended model (12 bands) with dielectric function correction (solid line) and without dielectric function correction (up triangle) up to 10 eV, standard model (eight bands) with correction.

$$\begin{aligned} R_{PA}(\hbar\omega) = 48\Gamma_{PA} \sum_{\mathbf{k},\mathbf{k}' \in IW} wW \sum_{l,u,i} \hbar\omega \\ \times \left[\sum_m \left| \frac{\langle m|\nabla_i|u\rangle}{E_u - E_m - \hbar\omega + i\Gamma_u} \right|^2 \right. \\ \left. + \sum_{m'} \left| \frac{\langle l|\nabla_i|m'\rangle}{E_{m'} - E_l - \hbar\omega + i\Gamma_u} \right| \right]^2 H^{ep}\sqrt{\epsilon} \\ \times \left| 1 + \frac{\omega}{\sqrt{\epsilon}} \frac{d\sqrt{\epsilon}}{d\omega} \right| f_u \bar{f}_l, \end{aligned} \tag{14}$$

where $i = 1,2,3$ are the photon polarization directions, w and W are the weights for the summation over the **k** points in IW. In the summation over u and l only the eigenstates with $|E_u - E_i - \hbar\omega \pm \hbar\omega_p| < \Delta E/2$ are considered.

The calculations are performed in SI units and R is then expressed in photons/(eV s m^{3}str). The results reported here are always expressed in these absolute units.

III. ANALYSIS OF THE PE RATE

Both the terms contribute to the total PE rate depending on the distribution function $f(E)$ and terms related to the band structure of the material and to the interaction Hamiltonian, through the matrix elements of Eq. (1).

The effects of the band structure on the PE rate can be studied by means of a band-coupling term defined as follows:

$$\Lambda(\hbar\omega) = \Gamma_{dir} \sum_{\mathbf{k} \in IW} \sum_{l,u} w\sqrt{\epsilon} \left| 1 + \frac{\omega}{\sqrt{\epsilon}} \frac{d\sqrt{\epsilon}}{d\omega} \right|. \tag{15}$$

The expression in Eq. (15) includes features related only to the band structure: the dielectric function and the DoS (summation over the band index for each **k** point). Figure 3 reports Λ as a function of the photon energy computed with the standard (eight bands) and the extended (12 bands) models. The triangles refer to the extended model without the corrections to the optical density of states due to the variability of the dielectric function with energy proposed in Ref. 20.

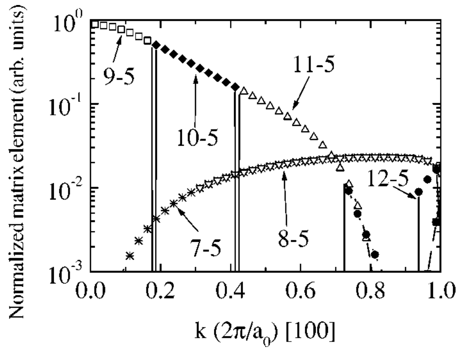

FIG. 4. Matrix elements calculated between two different bands with 46 361 **k** points in the IW. The transition is from an upper band to the first conduction band (cb). Upper band is third cb (star, 7-5), fourth (down triangle, 8-5), fifth (square, 9-5), sixth (diamond, 10-5), seventh (up triangle, 11-5), eighth (circle, 12-5). Even all the other possible transitions show that the fifth cb contribution is mostly dominant over wide ranges of **k** space.

The contribution of the four upper bands is weakly dependent on the photon energy, as expected from the almost flat density of states above approximately 8 eV (Ref. 21). The corrections proposed by Villa *et al.*[20] give rise to marked structures above approximately 3 eV. The maximum of Λ is at about 4.4 eV; assuming a constant occupation probability this fact would promote PE at this energy.

As for the matrix elements $|H_{lu}^{ef}|^2 = |\langle l|H^{ef}|u\rangle|^2$, Fig. 4 reports those pertinent to the first conduction band as a function of **k** along the direction $\langle 100\rangle$.

The dominant coupling terms along this **k**-space direction appear to be those related to the fifth conduction band. Since the fifth band extends from about 6.3 eV to 11.7 eV, i.e., in an energy range definitely accessible to electrons in tunneling experiments with MOS capacitors, these results reinforce the need to extend the band structure to higher energies as has been done in the present work. The matrix elements in other **k**-space directions show a qualitatively similar behavior but their absolute values are strongly dependent on the absolute values of **k**.

A. Phonon model

The phonon model used in this work is the same as the full band Monte Carlo (FBMC) described in Ref. 32 where it was proved to match experimental velocity and quantum yield data.

The deformation potentials are calculated in Ref. 20 as the product of an isotropic coupling constant and an analytic overlap factor depending on the exchanged kinetic momentum. Tests carried out by keeping the overlap factor according to Ref. 20 differ a little from the ones reported in this work (the overlap factor was assumed equal to the unit) only in the region 2–5 eV. The assumption of a constant overlap factor was kept in this work to put the phonon model in agreement with the MC terms.

Since the final state may fall outside the IW, the PE rate is multiplied for the 48-fold symmetry factor [see Eq. (14)]. The contribution of *f*-type and *g*-type phonons to the PE rate

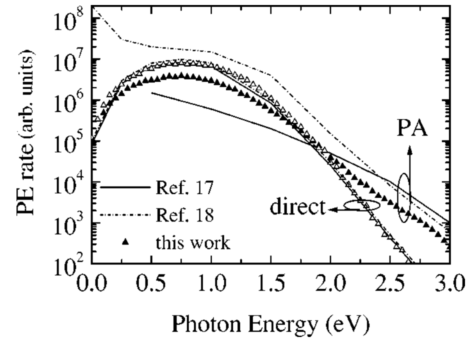

FIG. 5. Direct and PA photon emission rate related to the Gaussian distribution described in the text. Comparison between Bude *et al.* (Ref. 19) (solid line), Villa *et al.* (Ref. 20) (dashed-dotted line) and this work (triangle).

is multiplied by a factor of 1/6 and 4/6, respectively, so as to account for the band multiplicity.

The total PE rate for indirect PA transitions is obtained by simply summing the PE rates for each phonon type.

B. Model verification

The model has been tested comparing direct (*D*) and PA spectra with the results in Refs. 19 and 20. Figure 5 reports the emission spectra due to direct and PA *c*-*c* transitions calculated for a Gaussian distribution and the results showed in the references above for the same carrier distribution. The Gaussian distribution is represented empirically by the function $f(E) = N(A,B,n)\exp(-AE - BE^2)$; fixing the terms A and B at the values -1.82 and 1.41, respectively, the normalization factor is calculated as in Ref. 19 taking a carrier concentration of 10^{24} m^{-3}.

Excellent agreement with the results in Refs. 19 and 20 is found for *D*-type transitions. As for PA ones our model lies in between those of Ref. 19 and Ref. 20. The lower effective temperature for curves of this work and in Ref. 20 are due to the energy dependence of the dielectric function.

Figure 6 compares the *c*-*v* phonon-assisted spectra of our model with results in Ref. 19. Once again good mutual agreement is observed; discrepancies near band gap are likely due to the different energy discretization step at lower energies. Since only relative emission values have been published in Ref. 19, for the sake of a fair comparison their spectra have been multiplied for the same constant value in

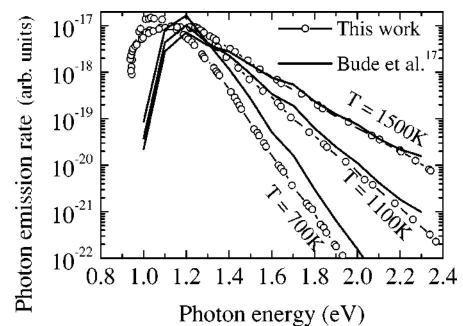

FIG. 6. Phonon-assisted PE rate for *c*-*v* transitions according to our model (solid lines) and simulations from Ref. 19 (symbols).

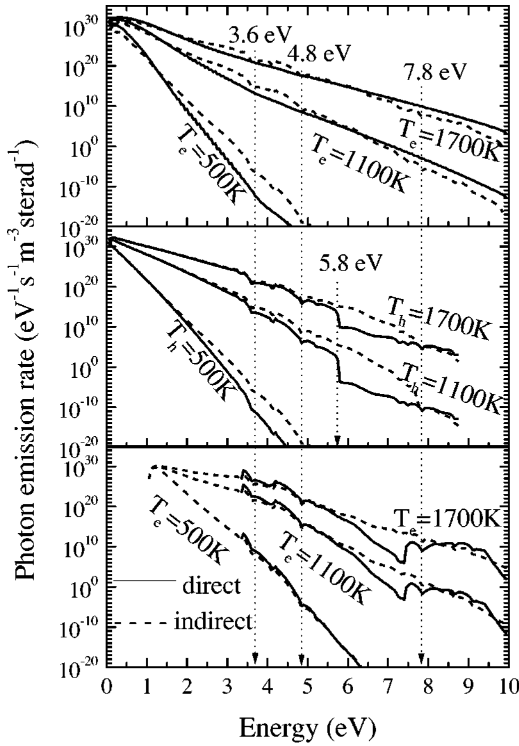

FIG. 7. PE rate for c-c (a), v-v (b), and c-v (c) direct (solid line) and PA (dotted line) transitions corresponding to Maxwellian distributions at several effective carrier temperatures (T_e, T_h).

both Figs. 5 and 6. These results confirm the validity of the model and its implementation.

IV. REMARKS ON THE PE RESULTS

Absolute photon emission rates integrated over the whole solid angle [i.e., in units of photons/(eV s m^{3}str)] for very different carrier distribution functions $f(E)$ (Mawellian, Gaussian, and Dirac's deltalike) were computed with the model and scaled to a reference carrier concentration of 10^{24} m^{-3}. Figure 7 reports the PE spectra due to the direct and all the total indirect (PA) c-c, v-v, and c-v transitions corresponding to Maxwellian distributions. The indirect PE rate represents the sum over all the phonon-type contributions cited in Sec. III A. The effective temperature T_h of the hole distribution in c-v spectra is 300 K.

At a lower energy (approximately 1 eV) the absolute values of PE rates for D and PA c-c and v-v transitions are comparable, but the slope of the PA spectra is slightly lower so that the two contributions cross each other at a higher energy (2–5 eV). PA emission rates exhibit structures at 3.6, 4.8, and 7.8 eV, clearly related to a corresponding sharp decrease of Λ (see Fig. 3).

Consistently with the results of Ref. 19 for a given T_e the direct PE rate has a higher slope than the PA one.

As for direct v-v-type transitions, a sharp reduction is observed around 5.8 eV, due to the corresponding decrease of the valence band DoS; PA curves do not show this effect because the scattering is calculated between the initial and final states and then the DoS behavior is averaged over the couple of these states.

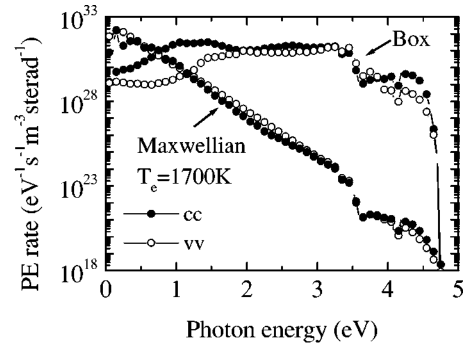

FIG. 8. c-c and v-v PA PE rate for Maxwellian and box (deltalike) distribution. The box is centered at 4.5 eV and is 0.5 eV wide.

As for c-v transitions, the D-type ones contribute only above approximately 3.5 eV, in good agreement with direct silicon band-gap values. The broad bump of the indirect PE rate above 7.3 eV is due to the increase in Λ, which is more evident in Fig. 3.

Figure 8 compares c-c and v-v PA transitions for two significantly different distribution functions normalized to the same carrier concentration 10^{24} m^{-3}: a heated Maxwellian and a Dirac's delta distribution, defined as a box function 0.5 eV wide centered around 4.5 eV. We see that over most of the explored energy range the photon spectra are very similar to each other. This implies that the relevant contribution of these two emission mechanisms in real devices is mostly determined by the relative carrier concentrations.

V. COMPARISON BETWEEN IMPACT IONIZATION AND PHOTON EMISSION SCATTERING RATES

In order to explain the origin of the substrate current in silicon devices under different bias conditions, the efficiency of impact ionization and photon emission in generating electron-hole pairs have to be compared.

To this purpose, we first restrict our analysis to hot-electron-induced photon emission (hence to devices as n-channel MOSFET's or npn BJT's); then we define a suitable scattering rate for hot-electron-induced photon emission as the probability (per unit of time) for one electron to generate a photon with energy higher than the energy gap (E_G), thus able to generate an electron-hole pair (if the photon is reabsorbed in the substrate). For an electron with energy E, this scattering rate is defined as

$$SR_{ph}(E)=\frac{4\pi\int_{E_G}^{\infty}[R_{dir}(\hbar\omega)+R_{PA}(\hbar\omega)]d\hbar\omega}{D_E\Delta E}, \quad (16)$$

where R_{dir} and R_{PA} are the emission spectra corresponding to a boxlike shaped electron distribution of width ΔE centered in E. D_E is the density of state for electrons in the conduction band and the factor 4π accounts for uniform radial emission in the whole solid angle.

As for impact ionization, the scattering rates for electrons and holes were evaluated following Ref. 33 and using the same extended band structure used in the previous photon

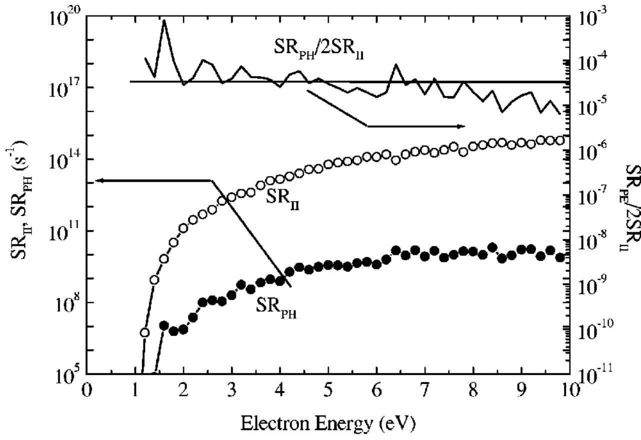

FIG. 9. Scattering rate for II and PE with $E>1.12$ eV through direct and PA *c*-*c* transitions.

emission calculations. The momentum conservation was satisfied over the carriers (primary and final electrons and holes) that are present in the process. A **k**-independent matrix element was used as a free parameter to reproduce the scattering rates reported in Ref. 34 for energies lower than 6 eV. As described in Ref. 35 the calculated scattering rate can reproduce quantum yield measurements in MOS capacitors over a wide range of bias voltages.

The lower part of Fig. 9 shows the electron-impact ionization scattering rate and the photon emission scattering rate due to *c*-*c* transitions. Both of them exhibit an energy threshold at the band-gap energy E_G and tend to saturate at higher energies.

To assess quantitatively the relative importance of impact ionization and photon emission as generation mechanisms of carrier pairs in the substrate we note that in saturated MOSFET's and tunneling MOS capacitors the hottest carriers (i.e., those responsible for the largest emission and ionization) are found in proximity of the Si-SiO_2 interface and that only photons emitted in the half solid angle oriented towards the substrate have a chance to be reabsorbed and to generate carrier pairs therein. Furthermore, we remind that the pair generation efficiency of photons with energy above the band gap is essentially equal to one.[36,37] Therefore, the maximum pair generation efficiency through photon emission processes can be quantified by half of the scattering rate of Eq. (16).

The upper part of Fig. 9 shows the ratio between half of the photon emission rate of Eq. (16) and the impact ionization scattering rate calculated with the extended band structure. This ratio has a weakly-energy-dependent value of $1-3\times10^{-5}$ that provides a simple physical explanation of the weakly-bias-dependent ratio of $\approx2\times10^{-5}$ between majority and minority substrate currents measured by many authors[13,16,38] in saturated *n*-MOSFET's.

For tunneling MOS capacitors biased under positive gate voltage, holes generated by impact ionization in the gate must cross the Si-SiO_2 barrier in order to be measurable at the substrate contact. If, following Ref. 6, we denote T_P the probability of these holes to be injected back in the substrate and measured as substrate current, we can approximate the ratio between the substrate current components due to reabsorption of photons ($I_{SUB,PH}$) and to anode hole injection ($I_{SUB,AHI}$) as

$$\frac{I_{SUB,PH}}{I_{SUB,AHI}}\approx\frac{SR_{PH}}{2SR_{II}T_P}. \tag{17}$$

Therefore the ratio between the photon emission and impact ionization scattering rates sets a lower boundary to the probability of hot hole injection that makes anode hole injection (AHI) the dominant hole generation mechanism in the substrate. In other words, the substrate current is dominated by photon emission reabsorption only if $T_P<3\times10^{-5}$. As described in Ref. 22, for oxide thicknesses and gate voltages in the range measured in Ref. 6, T_P is much higher than 3×10^{-5} and depends only weakly on oxide thickness and gate voltage. Thus we conclude that the correlation between I_{Smaj} and I_{Smin} measured in Ref. 6 can be explained by the weak energy dependence of T_P and SR_{PH}/SR_{II} (Fig. 9), without assuming that I_{Smaj} is dominated by photon emission-absorption processes.

VI. CONCLUSIONS

Nonlocal pseudopotential silicon band structure calculations have been extended up to significantly higher energies and compared with first-principle calculations. Results have been used to develop an extended model of spontaneous photon emission in silicon, fully consistent with the band structure and with the established transport model of an available Monte Carlo simulator for electron devices and including contributions from valence-to-valence band transitions.

Results compare favorably with previous reports in the literature and allow for an accurate comparison of impact ionization and photon emission as sources of carrier pairs in the substrate of silicon devices. A lower boundary of approximately 10^{-5} is established for the anode hole injection probability, which makes impact ionization and anode hole injection the dominant sources of holes and substrate current in tunneling MOS capacitors.

ACKNOWLEDGMENTS

The authors would like to thank Alberto Dalla Serra for support in performing the simulations of this work and Franco Venturi for the NL-EPM band calculation program and for helpful discussions and suggestions. This work was partially funded by Philips Research Laboratories, Einhoven, the Italian MURST (PRIN program) and CNR (5% and Madess II projects).

[1] A. Toriumi, M. Yoshimi, M. Iwase, Y. Akiiama, and K. Taniguchi, IEEE Trans. Electron Devices **34**, 1501 (1987).
[2] L. Selmi, Microelectron. Eng. **28**, 250 (1995).
[3] E. Cartier, J.C. Tsang, M.V. Fischetti, and D.A. Buchanan, Microelectron. Eng. **36**, 103 (1997).
[4] K. deKort and P. Damink, Proceedings of the European Sympsosium on Reliability of Electron Devices, Failure Physics and Analysis (unpublished), p. 45.
[5] K. deKort, P. Damink, and H. Boots, Phys. Rev. B **48**, 11 912 (1993).
[6] M. Rasras, I. DeWolf, G. Groeseneken, B. Kaczer, G. Degraeve, and H. Maes, *IEDM Technical Digest* (IEEE, Washington, 1999), p. 465.
[7] L. Selmi, M. Pavesi, H.-S.P. Wong, A. Acovic, and E. Sangiorgi, IEEE Trans. Electron Devices **45**, 1135 (1998).
[8] J.C. Tsang, J.A. Kash, and D.P. Vallet, IBM J. Res. Dev. **44**, 583 (2000).
[9] B. Eitan and A. Kolodny, Appl. Phys. Lett. **43**, 106 (1983).
[10] Z.A. Weinberg and M.V. Fischetti, J. Appl. Phys. **57**, 443 (1985).
[11] I.C. Chen, S.E. Holland, and C. Hu, J. Appl. Phys. **61**, 4544 (1987).
[12] K. F. Schuegraf and C. Hu, Proceedings of the International Reliability Physics Symposium (unpublished), p. 7.
[13] S. Tam and C. Hu, IEEE Trans. Electron Devices **31**, 1264 (1983).
[14] S. Kohyama, T. Furuyama, S. Mimura, and H. Iizuka, Jpn. J. Appl. Phys. **19**, 85 (1980).
[15] P.A. Childs, W. Eccleston, and R.A. Stuart, Electron. Lett. **17**, 281 (1981).
[16] P.A. Childs, R.A. Stuart, and W. Eccleston, Solid-State Electron. **26**, 685 (1983).
[17] A. Roy, R. Kazerounian, A. Kablanian, and B. Eitan, Proceedings of the International Reliability Physics Symposium (unpublished), p. 68.
[18] K. Kobayashi, A. Teramoto, M. Hirayama, and Y. Fujita, J. Appl. Phys. **77**, 3277 (1995).
[19] J. Bude, N. Sano, and A. Yoshii, Phys. Rev. B **45**, 5848 (1992).
[20] S. Villa, A.L. Lacaita, and A. Pacelli, Phys. Rev. B **52**, 10 993 (1995).
[21] P.L. Rigolli, M. Pavesi, M. Manfredi, P. Palestri, and L. Selmi (unpublished).
[22] P. Palestri, M. Pavesi, P. Rigolli, L. Selmi, A. Dalla Serra, A. Abramo, F. Widdershoven, and E. Sangiorgi, *IEDM Technical Digest* (IEEE, San Francisco, 2000), p. 97.
[23] J.R. Chelikowsky and M.L. Cohen, Phys. Rev. B **14**, 556 (1976).
[24] M. Bockstedte, A. Kley, J. Neugebauer, and M. Scheffler, Comput. Phys. Commun. **107**, 187 (1997).
[25] H.J. Monkhorst and J.D. Pack, Phys. Rev. B **13**, 5188 (1976).
[26] M. Fuchs and M. Scheffler, Comput. Phys. Commun. **119**, 67 (1999).
[27] H.S. Wong, *IEDM Technical Digest* (IEEE, Washington, 1991), p. 549.
[28] L. Selmi, H.S. Wong, M. Lanzoni, E. Sangiorgi, and M. Manfredi, *IEDM Technical Digest* (IEEE, Washington, 1993), p. 531.
[29] A. Lacaita, F. Zappa, S. Bigliardi, and M. Manfredi, IEEE Trans. Electron Devices **40**, 577 (1993).
[30] L. Selmi, M. Mastrapasqua, D.M. Boulin, J.D. Bude, M. Pavesi, E. Sangiorgi, and M.R. Pinto, IEEE Trans. Electron. Devices **45**, 802 (1998).
[31] E.D. Palik, *Handbook of Optical Constants in Solids* (Academic Press, New York, 1985).
[32] F. Venturi and A. Ghetti, Proceedings of SISPAD 1997 (unpublished), p. 343.
[33] N. Sano and A. Yoshii, Phys. Rev. B **45**, 4171 (1991).
[34] J.D. Bude and M. Mastrapasqua, IEEE Trans. Electron Devices **16**, 439 (1995).
[35] P.P. Palestri, L. Selmi, M. Pavesi, F. Widdershoven, and E. Sangiorgi, Proceedings of SISPAD (IEEE, Seattle, 2000), p. 38.
[36] A.J. Tuzzolino, Phys. Rev. **134**, A205 (1963).
[37] V.S. Vavilov, J. Phys. Chem. Solids **8**, 223 (1959).
[38] L. Selmi and D. Esseni, IEEE Trans. Electron Devices **46**, 376 (1999).